A Cool, Nutrient-Enriched Eastern Equatorial Pacific During the Mid-Pleistocene Transition

Rebecca S. Robinson, Colin A. Jones, Roger P. Kelly, Patrick Rafter, Johan Etourneau, Philippe Martinez

AGU100 ADVANCING EARTH AND SPACE SCIENCE

Geophysical Research Letters

RESEARCH LETTER
10.1029/2018GL081315

A Cool, Nutrient-Enriched Eastern Equatorial Pacific During the Mid-Pleistocene Transition

Rebecca S. Robinson[1], Colin A. Jones[1], Roger P. Kelly[1], Patrick Rafter[2], Johan Etourneau[3], and Philippe Martinez[4]

[1]Graduate School of Oceanography, University of Rhode Island, Narragansett, RI, USA, [2]Department of Earth System Science, University of California, Irvine, Irvine, CA, USA, [3]Instituto Andaluz de Ciencias de la Tierra, CSIC-Universidad Granada, Granada, Granada, Spain, [4]UMR CNRS 5805 EPOC, Université de Bordeaux, UMR CNRS EPOC, Pessac, France

Abstract The emergence of high-amplitude, low-frequency glacial-interglacial cycles during the mid-Pleistocene climate transition (MPT; 800–1,200 ka) is associated with global cooling. In the eastern equatorial Pacific, sea surface temperatures cooled, and the upwelling-induced cold tongue expanded significantly during the MPT. Here we use sedimentary records of iron, biogenic silica, and nutrient-nitrogen consumption to evaluate biogeochemical changes hypothesized to accompany the cold tongue expansion. Our results suggest that the eastern equatorial Pacific of the MPT hosted surface waters with higher nitrate contents and biogenic silica production relative to the last 600 ka. Increased production occurred despite low iron supply. We attribute this to enhanced upwelling and nutrient enrichment of thermocline waters, both likely related to the northward migration of Southern Ocean fronts. The return of these fronts to their southward positions after the MPT may be associated with stronger drawdown of nutrients and, potentially, atmospheric CO_2 in the Southern Ocean.

Plain Language Summary As the Earth's climate cooled, it also experienced a change in the frequency of ice ages around a million years ago. Ice ages became more intense and longer. In the equatorial Pacific, the transition between these two climate states is marked by a temporary expansion of cold surface water that winds deliver from below. Here we use sedimentary records to show that the expanded cold region also hosted higher nutrient concentrations and boosted biological production. The reconstructed increase in nutrient concentrations is interpreted as both an increase in the rate of nutrient supply, likely related to stronger winds, and delivery of waters bearing a higher overall nutrient concentration. Together, this implies a short-term redistribution of nutrients in the ocean. These data also suggest that the equatorial Pacific that we think of today as cool and nutrient rich relative to the rest of the tropical Pacific is small relative to ~900,000 years ago as a result of this shift in the climate.

Key Points:
- Expansion of the equatorial Pacific cold tongue during the MPT accompanied expanded nutrient richness and higher export of biogenic silica
- The increases in production and nutrient availability are attributed to enhanced upwelling and nutrient enrichment of thermocline waters
- The nutrient enrichment stems from reorganization of oceanic nutrient distributions linked to migration of Southern Ocean fronts

Supporting Information:
- Supporting Information S1

Correspondence to:
R. S. Robinson,
rebecca_r@uri.edu

Citation:
Robinson, R. S., Jones, C. A., Kelly, R. P., Rafter, P., Etourneau, J., & Martinez, P. (2019). A cool, nutrient-enriched eastern equatorial Pacific during the mid-Pleistocene transition. *Geophysical Research Letters*, *46*, 2187–2195. https://doi.org/10.1029/2018GL081315

Received 13 NOV 2018
Accepted 30 JAN 2019
Accepted article online 5 FEB 2019
Published online 26 FEB 2019

1. Introduction

The mid-Pleistocene climate transition (MPT; 800–1,200 ka) represents a change to the pacing of Earth's climate, where the orbital frequencies of glacial cycles shifted from dominantly 41-kyr obliquity paced cycles to quasi-100-kyr cycles caused by a response to internal climate system forcings or feedbacks (Chalk et al., 2017; Clark et al., 2006; McClymont et al., 2013). The MPT is marked by global climate changes, including expansion of large polar ice sheets (Lisiecki & Raymo, 2005) and the extent of the polar oceans (Martinez-Garcia et al., 2010), cooling of sea surface temperatures (SSTs; Herbert et al., 2010; McClymont et al., 2013), increased aridity (Schefuss et al., 2003), and a marked weakening of glacial meridional overturning circulation (MOC) at ~900 ka (Pena & Goldstein, 2014). In the tropical Pacific, the MPT is characterized by cooling, an expanded cold tongue, and intensification of the zonal SST gradient across the Pacific between 1,000 and 800 ka (Dyez et al., 2016; Dyez & Ravelo, 2014; Lawrence et al., 2006; Liu & Herbert, 2004; McClymont & Rosell-Melé, 2005). At the termination of the MPT, the meridional SST gradient expanded, and a modern-sized cold tongue was established in the eastern equatorial Pacific (EEP) around 700 ka (Dyez et al., 2016).

The EEP is one of the most biologically productive regions on Earth (Pennington et al., 2006). The interplay of climatic variables, including local tropical atmospheric dynamics, high-latitude ice sheet expansion, and global greenhouse gas forcing, drives the physics associated with upwelling and controls the ultimate source and nutrient content of upwelled waters. Today, the nutrient-rich cold tongue (Figure 1) is sustained by

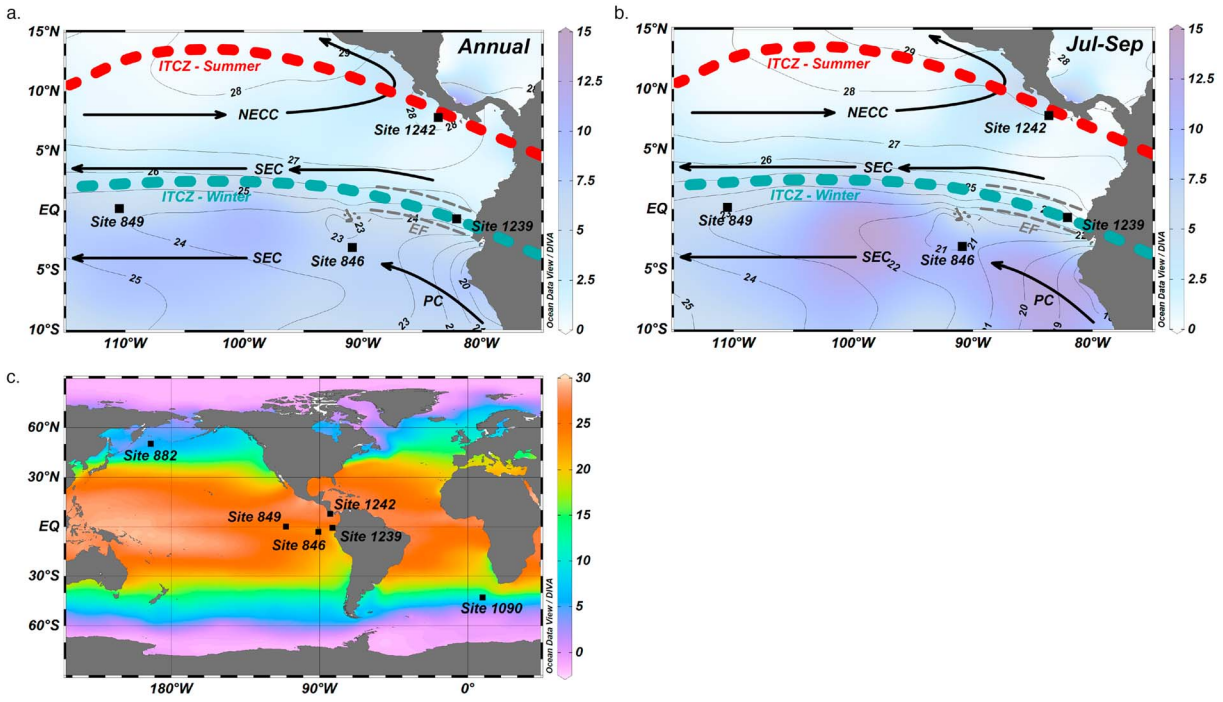

Figure 1. Maps of annual mean (a) and upwelling season (July–September) (b) surface nitrate (color scale, in μM) and sea surface temperature (contours, °C) in the eastern equatorial Pacific. A global map of mean annual sea surface temperature (c) highlights positions of all sites discussed in the text, including Ocean Drilling Program Sites 1090 and 882, located outside of the eastern equatorial Pacific. Data are from WOA13 (Garcia et al., 2014; Locarnini et al., 2013). In panels (a) and (b), surface ocean current locations, based on Kessler (2006), are shown in black arrows (SEC = South Equatorial Current; NECC = North Equatorial Counter Current; PC = Peru Current). The dashed black line marks the approximate position of the equatorial front (EF), while the broad dashed green line marks the winter Intertropical Convergence Zone (ITCZ) location, and the broad dashed red line marks the summer ITCZ location.

equatorial and coastal wind-driven upwelling. The strength of upwelling is regulated by the pole-to-equator temperature gradient, which is related to heat transport across the equator and the strength of the trade winds (Marshall et al., 2014; Mitchell & Wallace, 1992).

The modern Intertropical Convergence Zone (ITCZ) shifts seasonally, moving to its northernmost position during the boreal summer. The northward position is associated with the strongest cross-equatorial winds, intense upwelling, and cooling of the sea surface (Chelton et al., 2001). The east-west tilt of the thermocline (shoaling to the east) allows the upwelling systems to tap into cooler, nutrient rich waters that originate in the Southern Ocean (Lehmann et al., 2018; Toggweiler et al., 1991) and are modified, in terms of nutrient content and nitrogen isotopes, in route to the equator (Rafter et al., 2012, 2013). In the modern surface ocean, consumption of nitrate (the most abundant form of nutrient-nitrogen in the EEP) is limited by the availability of iron, both externally supplied and recycled, yet the degree of drawdown varies with upwelling strength (Rafter et al., 2017). Published sedimentary nitrogen isotope records from EEP Ocean Drilling Program (ODP) Sites 849, 1239, and 1240 show lower values, on average, during the MPT relative to the last 1 Ma (Etourneau et al., 2013; Rafter et al., 2012). These records generally are interpreted as recorders of changes in nutrient consumption associated with equatorial upwelling strength, which is suggested to track local insolation changes (Etourneau et al., 2013; Rafter & Charles, 2012). Here we present these existing records with new biogenic silica and sedimentary nitrogen isotope data from ODP Site 846 to ask whether the expanded cold tongue was associated with regional nutrient supply and demand changes across the MPT. The data suggest a potentially significant shift in upwelling and nutrient delivery to the EEP during this climate transition.

2. Methods

2.1. Study Sites and Materials

We present 310 new nitrogen isotope measurements and calibrated scanning X-ray fluorescence (XRF) silicon (Si) and iron (Fe) data from ODP Site 846 (3.1°S, 90.8°W, 3,000-m depth), located in the heart of the

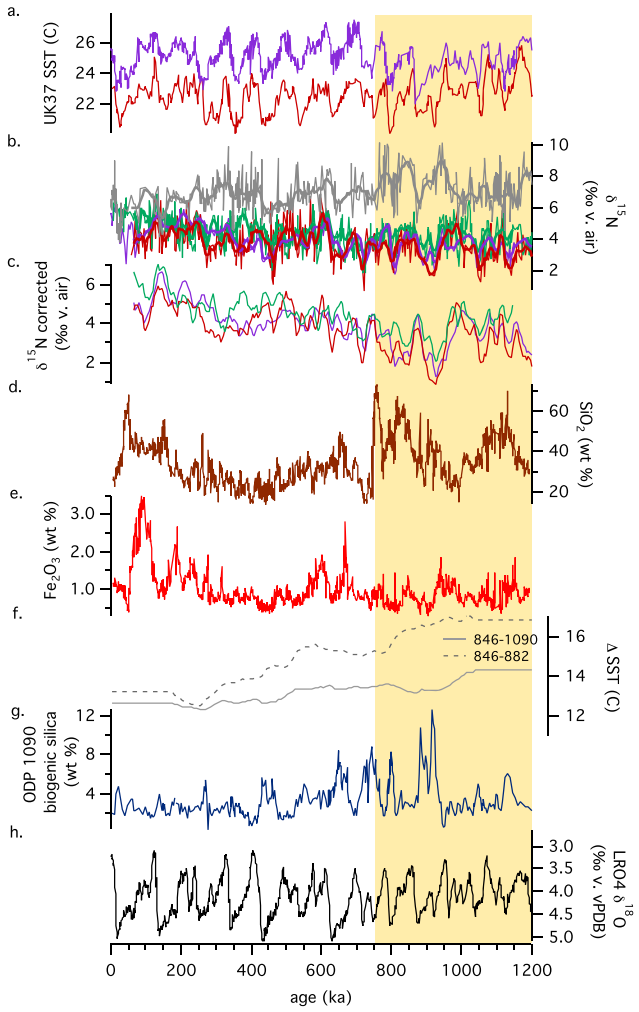

Figure 2. Eastern equatorial Pacific (EEP) records of nutrient consumption and Ocean Drilling Program (ODP) Site 846 biogenic silica and Fe_2O_3 records are compared to regional and global paleoclimate and paleoceanographic reconstructions. (a) Sea surface temperature (SST) at ODP Sites 1239 (purple) and 846 (red; Dyez et al., 2016; Etourneau et al., 2010); (b) bulk sedimentary $\delta^{15}N$ from ODP Sites 1239 (purple; Etourneau et al., 2013), 846 (red), 849 (green; Rafter et al., 2012), and 1242 (gray; Robinson et al., 2014). Bold lines reflect 3-pt running mean of each record after resampling at 5-kyr spacing. (c) Corrected $\delta^{15}N$ records from ODP Sites 1239 (purple), 846 (red), and 849 (green; see the supporting information for correction details). (d) Calibrated scanning X-ray fluorescence SiO_2 and (e) Fe_2O_3 (wt %) from ODP 846; (f) pole to equator SST gradients between subpolar North Pacific Site 882 and EEP Site 846 (dashed) and Subantarctic Site 1090 and EEP Site 846 (solid gray) line from Martinez-Garcia et al. (2010). (g) ODP Site 1090 biogenic silica (wt%; blue line) from Martinez-Garcia et al. (2011) and (h) LR04 global benthic oxygen isotope stack (Lisiecki & Raymo, 2005). The mid-Pleistocene climate transition interval of enhanced nutrient supply and export production to the EEP is highlighted by the yellow bar.

modern nitrate-rich, cold tongue, to study nutrient supply and demand dynamics and productivity, respectively (Figure 2). Site 846 data are presented on the Lawrence et al. (2006) age model. Age resolution of the nitrogen isotope record is approximately 4 kyr, while XRF measurements, taken at ~0.5-cm steps, provide subkiloyear resolution.

2.2. Discrete Measurements

Sedimentary nitrogen isotope values (as $\delta^{15}N$, where $\delta^{15}N = {}^{15}N/{}^{14}N_{sample}/{}^{15}N/{}^{14}N_{standard}-1$ and the universal standard is air) were determined on dried and ground sediment using a Costech 4010 Elemental Analyzer coupled to a Thermo Delta V isotope ratio mass spectrometer. $\delta^{15}N$ values are calibrated to the air reference value using reference materials IAEA N1 and N2 and an in-house aminocaproic acid standard. Precision was generally better than 0.3‰ (1σ value). Discrete measurements of biogenic silica for calibration of the XRF SiO_2 data were made using the molybdate blue colorimetric method (Mortlock & Froelich, 1989) after biogenic silica from ~25 mg of dried ground sediment was dissolved in 0.5-M sodium hydroxide and heated to 80 °C for 4 hr (Figure S1). Approximately 50% of the samples were measured at least twice, and these replicates were within ±3% of each other.

Inductively coupled plasma-mass spectrometry (ICP-MS) analyses were conducted to determine concentrations of Al_2O_3, $BaSO_4$, $CaCO_3$, TiO_2, MnO, and Fe_2O_3 in approximately 150 discrete samples for use in XRF calibration (Kelley et al., 2003). Briefly, dried ground sediment samples and standards were dissolved in nitric acid to dissolve $CaCO_3$. Remaining solids were dissolved successively in a 3:1 mixture of nitric acid and concentrated hydrofluoric acid, hydrochloric acid, and peroxides before 500,000× dilution in 5% nitric acid. Dilute samples were measured on a Thermo Quadrupole ICP-MS for trace metals in the Kelley Laboratory at the University of Rhode Island.

2.3. Scanning XRF Measurements and Calibration

Archive halves of sediment cores from ODP site 846 were measured for bulk composition on an Avaatech XRF Core Scanner at the IODP Gulf Coast Repository, College Station, Texas. Each core was scanned at 10 kV (800 uA, no filter, 20-s count time) for the lighter components (Al, Si, Ca, Ti, Mn, and Fe). Although only calibrated Si and Fe data are shown here, the six elements were used in the calibration. We applied a log-ratio calibration of the scanning XRF data, which accounts for matrix effects and nonlinear responses and incorporates a constant-sum constraint (Weltje & Tjallingii, 2008). For each possible pair of elements, reduced major axis regression was used to relate the log ratio of intensities of the element pair to the log ratio of ICP-MS standards of the element pair. Subsequently, the regression was used to calculate predicted log ratios for the standards from their matched XRF data. Goodness of fit for each element pair was assessed based on log-ratio residuals, and the element that reduced the median log-ratio standard deviation for all other elements was used as the common elemental ratio denominator. Finally, the regression that minimized residuals for each element was applied to the full XRF data set. Log ratios were converted to concentration by assuming full sediment component measurement (i.e., a constant-sum constraint) and normalizing to 100%. Weight percent (wt%) data may be biased because XRF cannot account for organic material (Lowemark et al., 2011; Weltje & Tjallingii, 2008); however, since the highest recorded organic carbon content in the last 1.5 Ma was 2% by weight (Shipboard-Scientific-Party, 1992), any overestimation for Site 846 is likely slight. Comparison of both weight percent and calculated mass

accumulation rate of discrete biogenic silica measurements (Figure S1 in the supporting information) supports interpretation of the high-resolution SiO_2 wt% record as a good measure of biogenic silica production. Moreover, the distinct pattern of Fe_2O_3, with overall lower values when SiO_2 is high, indicates that the SiO_2 is not siliciclastic in nature (Figure 2). Biogenic silica does not appear to be strongly influenced by variations in sediment accumulation rate either (Figure S1).

3. Results and Discussion

3.1. High-Resolution Nitrogen Isotope and Scanning XRF Data From ODP 846

The new ODP Site 846 records show relatively low sedimentary $\delta^{15}N$ and elevated biogenic silica accumulation centered around 900 ka, with low-frequency variability about the mean (Figure 2b, red line). Subsequently, $\delta^{15}N$ values progressively increased, and biogenic silica deposition decreased (Figure 2; Dyez et al., 2016). These data imply that EEP surface waters were nutrient rich and supported relatively high production of biogenic silica during the MPT followed by a transition toward lower nutrient and export conditions that persist today (Figure 2). This suggests that the expansion of the cold tongue was accompanied by significant biogeochemical changes during the MPT.

3.2. Nutrient Utilization Across the EEP

Compiling the Site 846 $\delta^{15}N$ data with other published sedimentary $\delta^{15}N$ records from the region—ODP Sites 849 (Rafter et al., 2012) and 1239 (Etourneau et al., 2013), presented on their published age models—implies that nutrient enrichment occurred throughout the EEP during the MPT (Figures 1 and 2). Before deeply interpreting the $\delta^{15}N$ data, they must be corrected for changes in the isotopic composition of nitrate in the source waters (Galbraith et al., 2008; Rafter & Charles, 2012; Robinson et al., 2009). Subsurface waters of the EEP are impacted by exchange with partially denitrified waters from within the eastern tropical Pacific oxygen minimum zone, and this exchange elevates the regional subsurface $\delta^{15}N$ value (Rafter et al., 2012; Robinson et al., 2009; Toggweiler et al., 1991). It has also been shown that the extent of pelagic denitrification varied in the past (Galbraith et al., 2013; Robinson et al., 2014). The sedimentary $\delta^{15}N$ record from ODP Site 1242, recovered from the eastern tropical north Pacific oxygen minimum zone, is a good monitor of the regional denitrification overprint (Robinson et al., 2009, 2014). We used the deviation from the 1,200-kyr mean $\delta^{15}N$ value at Site 1242 as an estimate of $\delta^{15}N$ variability attributable to pelagic denitrification. All records were smoothed and resampled at a 5-kyr interval. The measured bulk sedimentary $\delta^{15}N$ data from Sites 846, 849, and 1239 were corrected by subtracting the difference between the Site 1242 measured value at a given time step and the ODP Site 1242 1,200-kyr mean $\delta^{15}N$ value (6.2‰) from the $\delta^{15}N$ value at that same time step in the EEP records (see the supporting information for more details on the correction). With the variation in source removed, the corrected $\delta^{15}N$ values reflect changes in nutrient utilization in the nutrient rich EEP, where higher $\delta^{15}N$ values reflect more extensive consumption of the nitrate pool during photosynthesis as recorded by the resulting organic matter (Figure 2c). The corrected data for Site 846 show an amplification of the overall trend from lower $\delta^{15}N$ values during the MPT toward higher values centered around 500 ka. The correction increases the amplitude of the MPT to late Pleistocene difference in mean $\delta^{15}N$ by ~0.8‰ (Figures 2c and S2). Because all of the EEP data were treated identically, gradients between the sites are not impacted by the correction. A spatial $\delta^{15}N$ gradient did not emerge with the expanding SST gradient around 800 ka.

The corrected $\delta^{15}N$ data from ODP Sites 846, 849, and 1239 indicate that nitrate consumption across the EEP was significantly reduced between 700 and 1,200 ka when biogenic silica deposition at Site 846 was elevated (Figure 2d). While lower eolian Fe supply and associated Fe limitation of nitrate uptake could explain the lower $\delta^{15}N$ values during the MPT (Figure 2e; Winckler et al., 2005), it is unlikely. The increase in biogenic silica production requires that there was an increase in surface nutrient supply, since silicic acid is typically limiting to biogenic silica production the EEP (Brzezinski et al., 2011). The reduction in relative nutrient consumption reflected in the $\delta^{15}N$ data implies that the increase in nutrient supply must have exceeded the increase in demand indicated by biogenic silica peaks. The inferred increase in nutrient supply co-occurs with a regional SST decrease and a reduced meridional SST gradient in the EEP (Figure 2a; Dyez et al., 2016), indicating that the EEP hosted an expanded, nutrient-rich cold tongue during the MPT.

3.3. Causes of Higher Nutrient Supply During the MPT

Dyez et al. (2016) concluded that the increase of the meridional SST gradient after the MPT between ODP Sites 846 and 1239 was not related to changes in the intensity of upwelling but rather to warming at ODP Site 1239. Site 1239 lies very close to the modern equatorial front (EF; Figure 1), the boundary between the warm, nutrient-poor waters of the North Equatorial Counter Current (NECC) and the cold tongue. Because the NECC is nutrient poor, it contributes little nitrate relative to what is advected northward by the equatorial upwelling cells and does not have an impact on the $\delta^{15}N$ value of nitrate in the sea surface over Site 1239 or change the $\delta^{15}N$ gradient between Sites 846 and 1239. While a southward migration of the EF would warm and lower the nutrient content of the waters over Site 1239, it would not cause the increase in $\delta^{15}N$ observed at 700 ka. In addition, if a shift in the EF was the only cause of the expanding SST gradient, then productivity and nutrient supply should remain constant at ODP Site 846. However, the observed variations in biogenic silica production and nitrate supply associated with the SST fluctuations require changes in either the amount of upwelling or in the nutrient content of the upwelled water.

The position of the ITCZ and the intensity of upwelling have been mechanistically related to the MOC, through its net northward advection of heat and the compensating southward atmospheric heat transport by the southern Hadley cell (Donohoe et al., 2013; Marshall et al., 2014). The upwelling-inducing southeasterly trades are the lower limb of this Hadley cell, and they intensify as the ITCZ shifts northward (Donohoe et al., 2013). Thus, a weakening of the glacial MOC around 900 ka (Pena & Goldstein, 2014) should have resulted in reduced equatorial upwelling (Donohoe et al., 2013). This scenario is, however, difficult to reconcile with our new records, showing that nutrient supply and biogenic silica productivity instead peaked around 900 ka and remained relatively high throughout the MPT until ~700 ka.

Upwelling can also be enhanced by increased zonal temperature gradients and the resulting atmospheric circulation (i.e., strengthening of Walker Circulation). Previous studies suggest that the zonal temperature gradients in the EEP expanded to their present extent across the MPT (Dyez & Ravelo, 2014; Etourneau et al., 2010; McClymont & Rosell-Melé, 2005). This should progressively intensify upwelling post-MPT, opposite of our observations.

SST reconstructions from the EEP, together with western equatorial Pacific dust accumulation and source data, suggest a far northerly position of the ITCZ between 1,200 and 900 ka with a transition to its modern position between 900 and 700 ka (Dyez et al., 2016; Seo et al., 2015). Higher overall productivity and nutrient supply between 700 and 1,200 ka are consistent with enhanced, upwelling favorable, southeasterly trades during the MPT. A documented shift of meridional temperature gradients suggests that the pole-to-equator SST gradient was at its maximum around 900 ka; after which, it relaxed steadily until around 400 ka (Martinez-Garcia et al., 2010; Figure 2). The enhanced large-scale gradients are also consistent with enhanced upwelling. We note here that upwelling intensity is inherently difficult to reconstruct. It is fundamentally a wind-driven process that results in cooling of the sea surface and enhanced nutrient supply, two characteristics that are not uniquely related to upwelling. Here we provide evidence for both cooling and increased nutrient supply but acknowledge that evidence for enhanced winds (i.e., upwelling favorable winds) is lacking.

Nutrient supply to the EEP, and therefore productivity, is linked to the extra tropics by the thermocline (Loubere, 2000; Pena et al., 2008; Robinson et al., 2009; Spero & Lea, 2002). A decrease in the zonal tilt, the mean depth, or the nutrient content of the thermocline causes variation in nutrient supply to the EEP. As mentioned, the zonal temperature gradient, a manifestation of the zonal tilt of the thermocline, expanded toward its modern configuration during the MPT, and this gradient was maintained (Dyez & Ravelo, 2014; Etourneau et al., 2010; McClymont & Rosell-Melé, 2005). This implies that upwelling intensified after the MPT and that the nutricline was closer to the surface, potentially enriching the nutrient content of upwelled water. The post-MPT decrease in production that we observe, however, does not fit with this shift.

The mean depth of the thermocline is thought to shoal with an expansion of the polar oceans and contraction of the subtropics (Lawrence et al., 2013; Philander & Fedorov, 2003). The shift in the pole-to-equator temperature gradients (Martinez-Garcia et al., 2010), as well as the shifting of Southern Ocean fronts equatorward (Becquey & Gersonde, 2002; Kemp et al., 2010), implies that a contraction of low latitudes occurred

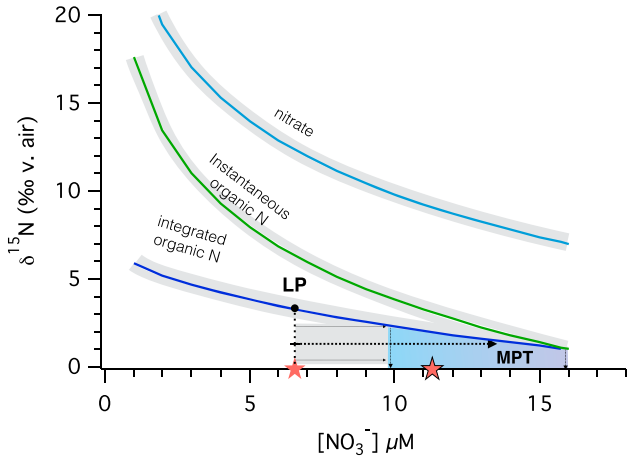

Figure 3. An approximation of the change in nitrate concentrations at site 846 between the late Pleistocene (LP) and the mid-Pleistocene climate transition (MPT), based on the relative change in $\delta^{15}N_{corrected}$, assuming a closed, Rayleigh-like fractionation of nitrate isotopes. Estimated [NO_3^-] are shown as vertical, dotted arrows for the LP (mean), MPT (mean), and MPT max cases. The red star marks mean annual [NO_3^-] above ODP Site 846, the outlined red star marks [NO_3^-] during boreal summer, the seasonal upwelling period. The ~2.0 ± 1.0‰ decrease in mean $\delta^{15}N$ values between the LP and MPT cases is depicted by a dashed vertical line between the solid black circle and the horizontal bar and it implies a mean increase in [NO_3^-] of approximately 3–9 μM (dashed horizontal arrows ± gray shading to blue box). The estimated MPT [NO_3^-] bracket the upwelling season [NO_3^-] above ODP Site 846 (outlined red star). The maximum estimated [NO_3^-] is at least 16 μM, close to the assumed upwelling source (15.8 ± 2.2 μM). Estimates are based on the modern [NO_3^-] and the relative changes in sedimentary $\delta^{15}N$ rather than the mean $\delta^{15}N$ values for a given time period. This is because we cannot account for sedimentary alteration of the $\delta^{15}N$ (Altabet & Francois, 1994; Robinson et al., 2012).

between 1.5 and 1.2 Ma and reached a minimum around 800–900 ka (Figure 2; Martinez-Garcia et al., 2010). The changes in pole-to-equator temperature gradients are consistent not only with enhanced upwelling but also with a shallow thermocline during the MPT, potentially resulting in the upwelling of water with a higher overall nutrient content.

The nutrient content of subsurface waters during the MPT may have been enriched relative to the present day. Nutrients available to the upwelling circulation in the EEP are largely from Subantarctic Mode Water, which is ultimately sourced in the Southern Ocean (Kessler, 2006; Sarmiento et al., 2004; Toggweiler et al., 1991). Higher opal burial at ODP Site 1090, in the Subantarctic Zone of the Southern Ocean between 1,200 and 700 ka, indicates that major nutrients, including silicic acid in the region of mode water formation, at the southern edge of the Subantarctic Zone and south of the Site 1090, were elevated during glacials between 1,200 and 700 ka (Figure 2; Martinez-Garcia et al., 2011). Micropaleontological-based reconstructions indicate a equatorward migration of the Southern Ocean fronts during the MPT that likely ushered higher nutrient content waters northward (Becquey & Gersonde, 2002; Flores & Sierro, 2007; Kemp et al., 2010), making them available for export to the low latitudes. An increase in the relative contributions of North Pacific intermediate water (NPIW), a secondary source of nutrients to the equatorial upwelling system, could also have increased the nutrient content of upwelled waters, and because NPIW is relatively silicate rich, this would explain the shift toward enhanced biogenic silica burial (Sarmiento et al., 2004). However, $\delta^{15}N$ records from the Subarctic Pacific where NPIW is formed suggest that the nutrient content of NPIW was likely lower as a result of enhanced utilization during the MPT, while ventilation was at least slightly weaker than post-MPT (Knudson & Ravelo, 2015a, 2015b).

3.4. Surface Nitrate Concentrations During the MPT

The $\delta^{15}N$ data present a regional picture of a very nitrate-rich EEP during the MPT. The nitrogen isotope data can be used to make first-order estimates of surface nitrate concentrations. Assuming a simple Rayleigh approximation of nutrient consumption, based on an integrated product formulation, a constant source of nitrate (~16 μM with $\delta^{15}N = 7.1 \pm 0.3$‰), a constant isotope effect (epsilon [ε] = 6‰; Rafter et al., 2017), and the integrated product formulation of Mariotti et al. (1981), we estimate that the ~2‰ difference in $\delta^{15}N$ values between the late Pleistocene mean $\delta^{15}N$ at ODP Site 846 (4.9 ± 0.5‰, 0–250 ka) and the mean $\delta^{15}N$ value during the MPT (2.9 ± 1‰, 700–1200 ka) implies mean nitrate concentrations at ODP Sites 846 during the MPT > 10 μM (Figure 3). Concentrations above 10 μM occur in the modern boreal summer during peak upwelling season (Figures 1 and 3). The lowest values, from 900 ka, imply a much greater increase in surface nitrate (to ~16 μM). This implies almost no nitrate depletion in the face of exceptionally high opal production if the upwelling concentrations remained the same. Although the enhanced meridional SST gradients likely intensified upwelling, the magnitude of the $\delta^{15}N$ shift may even *require* an increase in the nutrient content of the upwelled water.

4. Implications and Conclusions

Sedimentary $\delta^{15}N$ records from the EEP, with an accompanying high-resolution XRF record of biogenic silica, demonstrate significant nutrient enrichment of the cold tongue during the MPT. Nutrient enrichment of the surface ocean, despite significant nutrient requirements associated with high productivity, was driven by intensified upwelling and an increase in the nutrient content of the thermocline. Published time series analysis of the ODP Site 849 nutrient utilization record suggests that EEP upwelling was a near-linear response to insolation over the last million years. It diverges from its typical linear relation to insolation during the MPT, when insolation shows high-amplitude variability, but the nutrient utilization record

does not (Rafter et al., 2012). The transient reorganization of nutrient distributions that elevated nutrient supply to the EEP during the MPT disrupted the predictable insolation-driven variability of the equatorial ecosystem.

The expanded, nutrient-enriched cold tongue during the MPT also implies that the modern EEP cold tongue is diminished relative to the early Pleistocene and the contraction of this oceanic system occurs with the shift to the 100 kyr, high-amplitude glacial cycles. The expansion and subsequent contraction of this ecosystem were due, at least in part, to a spatial redistribution of nutrients, both vertically and horizontally, in the global ocean. These changes have implications for the global carbon cycle and are likely linked to the changing climate across the MPT.

The available reconstructions indicate that atmospheric CO_2 concentrations during glacial periods decreased after the MPT (Chalk et al., 2017; Hönisch et al., 2009). During the MPT, the weak nutrient consumption implied by the $\delta^{15}N$ records presented here suggests that despite high biogenic silica burial, the EEP was a local source of CO_2 to the atmosphere. More importantly for the global air-sea CO_2 balance (Marinov et al., 2006; Sigman et al., 2010), the inference of higher nutrient supply to the low latitudes suggests that the biological pump south of the Polar Front was relatively weak during the MPT. After the MPT, the reduction in pCO_2 is attributed to an enhanced Southern Ocean biological pump stimulated by enhanced Fe availability as a result of the increased aridity and dustiness of the atmosphere (Chalk et al., 2017; Martinez-Garcia et al., 2011). The decrease in nutrient supply to low latitudes suggests that nutrient drawdown in the polar Antarctic ramped up across the MPT, consistent with the inferred Fe fertilization of the post-MPT polar oceans (Chalk et al., 2017). Downstream in the EEP, the diminished supply of nutrients from the Southern Ocean and the contraction of the cold tongue (Dyez et al., 2016) resulted in the carbonate-dominated ecosystem that exists today.

Acknowledgments
This work was supported in part by NSF-MGG (1060779) and USSSAC postcruise support for Leg 202 to R. S. R. We thank P. Rumford and the IODP Core repository for providing samples and assistance with XRF core scanning; K. Kelley for analytical assistance; and Z. Kerrigan, J. Freedman, and A. Stahl for the help with sample preparation. New data will be archived at the NCEI Paleoceanography Data Repository. Supporting information for this paper is available.

References

Altabet, M. A., & Francois, R. (1994). Sedimentary nitrogen isotopic ratio as a recorder for surface nitrate utilization. *Global Biogeochemical Cycles*, *8*(1), 103–116. https://doi.org/10.1029/93GB03396

Becquey, S., & Gersonde, R. (2002). Past hydrographic and climatic changes in the Subantarctic Zone of the South Atlantic—The Pleistocene record from ODP site 1090. *Palaeogeography Palaeoclimatology Palaeoecology*, *18*(3-4), 221–239. https://doi.org/10.1016/S0031-0182(01)00497-7

Brzezinski, M. A., Baines, S. B., Balch, W. M., Beucher, C. P., Chai, F., Dugdale, R. C., et al. (2011). Co-limitation of diatoms by iron and silicic acid in the equatorial Pacific. *Deep-Sea Research Part II*, *58*, 493–511. https://doi.org/10.1016/j.dsr2.2010.08.005

Chalk, T. B., Hain, M. P., Foster, G. L., Rohling, E. J., Sexton, P. F., Badger, M. P. S., et al. (2017). Causes of ice age intensification across the mid-Pleistocene transition. *Proceedings of the National Academy of Sciences of the United States of America*, *114*, 13,114–13,119. https://doi.org/10.1073/pnas.1702143114

Chelton, D. B., Esbensen, S. K., Schlax, M. G., Thum, N., Freilich, M. H., Wentz, F. J., et al. (2001). Observations of coupling between surface wind stress and sea surface temperature in the Eastern Tropical Pacific. *Journal of Climate*, *14*(7), 1479–1498. https://doi.org/10.1175/1520-0442(2001)014<1479:OOCBSW>2.0.CO;2

Clark, P. U., Archer, D., Pollard, D., Blum, J. D., Rial, J. A., Brovkin, V., et al. (2006). The middle Pleistocene transition: Characteristics, mechanisms, and implications for long-term changes in atmospheric pCO2. *Quaternary Science Reviews*, *25*, 3150–3184. https://doi.org/10.1016/j.quascirev.2006.07.008

Donohoe, A., Marshall, J., Ferreira, D., & McGee, D. (2013). The relationship between ITCZ location and cross-equatorial atmospheric heat transport: From the seasonal cycle to the last glacial maximum. *Journal of Climate*, *26*, 3597–3618. https://doi.org/10.1175/JCLI-D-12-00467.1

Dyez, K. A., & Ravelo, A. C. (2014). Dynamical changes in the tropical Pacific warm pool and zonal SST gradient during the Pleistocene. *Geophysical Research Letters*, *41*, 7626–7633. https://doi.org/10.1002/2014GL061639

Dyez, K. A., Ravelo, A. C., & Mix, A. C. (2016). Evaluating drivers of Pleistocene eastern tropical Pacific sea surface temperature. *Paleoceanography*, *31*, 1054–1069. https://doi.org/10.1002/2015PA002873

Etourneau, J., Robinson, R. S., Martinez, P. M., & Schneider, R. (2013). Large changes in upwelling intensity, biological production and nutrient utilization in the Eastern Equatorial Pacific over the last 3. 2 Ma. *Biogeosciences*, *10*, 5663–5670. https://doi.org/10.5194/bg-10-5663-2013

Etourneau, J., Schneider, R., Blanz, T., & Martinez, P. (2010). Intensification of the Walker and Hadley atmospheric circulations during the Pliocene-Pleistocene climate transition. *Earth and Planetary Science Letters*, *297*, 103–110. https://doi.org/10.1016/j.epsl.2010.06.010

Flores, J., & Sierro, F. J. (2007). Pronounced mid-Pleistocene southward shift of the polar front in the Atlantic sector of the Southern Ocean. *Deep-Sea Research Part II*, *54*, 2432–2442. https://doi.org/10.1016/j.dsr2.2007.07.026

Galbraith, E., Kienast, M., & Group, N.W (2013). The acceleration of oceanic denitrification during deglacial warming. *Nature Geoscience*, *6*, 579–584. https://doi.org/10.1038/NGEO1832

Galbraith, E. D., Kienast, M., Jaccard, S. L., Pedersen, T. F., Brunelle, B. G., Sigman, D. M., & Kiefer, T. (2008). Consistent relationship between global climate and surface nitrate utilization in the western subarctic Pacific throughout the last 500 ka. *Paleoceanography*, *23*, PA2212. https://doi.org/10.1029/2007PA001518

Garcia, H. E., Locarnini, R. A., Boyer, T. P., Antonov, J. I., Baranova, O. K., Zweng, M. M., et al. (2014). World Ocean Atlas 2013, Volume 4: Dissolved Inorganic Nutrients (phosphate, nitrate, silicate). In S. Levitus & A. Mishonov (Eds.), *NOAA Atlas NESDIS 76* (25 pp.).

Herbert, T. D., Peterson, L. C., Lawrence, K. T., & Liu, Z. (2010). Tropical ocean temperatures over the past 3.5 million years. *Science*, *328*, 1530–1534. https://doi.org/10.1126/science.1185435

Hönisch, B., Hemming, N. G., Archer, D., SIddall, M., & McManus, J. (2009). Atmospheric carbon dioxide concentration across the mid-Pleistocene transition. *Science*, *324*, 1552–1554. https://doi.org/10.1126/science.1171477

Kelley, K. A., Plank, T., Ludden, J., & Staudigel, H. (2003). Composition of altered oceanic crust at ODP sites 801 and 1149. *Geochemistry, Geophysics, Geosystems*, *4*(6), 8910. https://doi.org/10.1029/2002GC000435

Kemp, A. E. S., Grigorov, I., Pearce, R. B., & Naveira Garabato, A. C. (2010). Migration of the Antarctic polar front through the mid-Pleistocene transition: Evidence and climatic implications. *Quaternary Science Reviews*, *29*(17-18), 1993–2009. https://doi.org/10.1016/j.quascirev.2010.04.027

Kessler, W. S. (2006). The circulation of the eastern tropical Pacific: A review. *Progress in Oceanography*, *69*(2-4), 181–217. https://doi.org/10.1016/j.pocean.2006.03.009

Knudson, K. P., & Ravelo, A. C. (2015a). Enhanced subarctic Pacific stratification and nutrient utilization during glacials over the last 1.2Myr. *Geophysical Research Letters*, *42*, 9870–9879. https://doi.org/10.1002/2015GL066317

Knudson, K. P., & Ravelo, A. C. (2015b). North Pacific intermediate water circulation enhanced by the closure of the Bering Strait. *Paleoceanography*, *30*, 1287–1304. https://doi.org/10.1002/2015PA002840

Lawrence, K. T., Liu, Z., & Herbert, T. D. (2006). Evolution of the eastern tropical Pacific through Plio-Pleistocene glaciation. *Science*, *312*, 79–83. https://doi.org/10.1126/science.1120395

Lawrence, K. T., Sigman, D. M., Herbert, T. D., Riijimaki, C. A., Bolton, C. T., Martinez-Garcia, A., et al. (2013). Time-transgressive North Atlantic productivity changes upon Northern Hemisphere glaciation. *Paleoceanography*, *28*, 740–751. https://doi.org/10.1002/2013PA002546

Lehmann, N., Granger, J., Kienast, M., Brown, K. S., Rafter, P. A., Martinez- Mendez, G., & Mohtadi, M. (2018). Isotopic evidence for the evolution of subsurface nitrate in the Western Equatorial Pacific. *Journal of Geophysical Research: Oceans*, *123*, 1684–1707. https://doi.org/10.1002/2017JC013527

Lisiecki, L. E., & Raymo, M. E. (2005). A Pliocene-Pleistocene stack of 57 globally distributed benthic d18O records. *Paleoceanography*, *20*, PA1003. https://doi.org/10.1029/2004PA001071

Liu, Z. H., & Herbert, T. D. (2004). High-latitude influence on the eastern equatorial Pacific climate in the early Pleistocene epoch. *Nature*, *427*, 720–723. https://doi.org/10.1038/nature02338

Locarnini, R. A., Mishonov, A. V., Antonov, J. I., Boyer, T. P., Garcia, H. E., Baranova, O. K., et al. (2013). World Ocean Atlas 2013, Volume 1: Temperature. In S. Levitus & A. Mishonov (Eds.), *NOAA Atlas NESDIS 73* (40 pp.).

Loubere, P. (2000). Marine control of biological production in the eastern equatorial Pacific Ocean. *Nature*, *406*(6795), 497–500. https://doi.org/10.1038/35020041

Lowemark, L., CHen, H.-F., Yang, T.-N., Kylander, M., Yu, E.-F., Hsu, Y.-W., et al. (2011). Normalizing XRF-scanner data: A cautionary note on the interpretation of high-resolution records from organic-rich lakes. *Journal of Asian Earth Sciences*, *40*, 1250–1256. https://doi.org/10.1016/j.jseaes.2010.06.002

Marinov, I., Gnanadesikan, A., Toggweiler, J. R., & Sarmiento, J. L. (2006). The Southern Ocean biogeochemical divide. *Nature*, *441*, 964–967. https://doi.org/10.1038/nature04883

Mariotti, A., Germon, J. C., Hubert, P., Kaiser, P., Letolle, R., Tardieux, A., & Tardieux, P. (1981). Experimental determination of nitrogen kinetic isotope fractionation: Some principles; illustration for the denitrification and nitrification processes. *Plant and Soil*, *62*(3), 413–430. https://doi.org/10.1007/BF02374138

Marshall, J., Donohoe, A., Ferreira, D., & McGee, D. (2014). The ocean's role in setting the mean position of the Inter-Tropical Convergence Zone. *Climate Dynamics*, *42*, 1967–1979. https://doi.org/10.1007/s00382-013-1767-z

Martinez-Garcia, A., Rosell-Melé, A., Jaccard, S. L., Geibert, W., Sigman, D. M., & Haug, G. H. (2011). Southern Ocean dust-climate coupling over the past four million years. *Nature*, *476*, 312–315. https://doi.org/10.1038/nature10310

Martinez-Garcia, A., Rosell-Mele, A., McClymont, E. L., Gersonde, R., & Haug, G. H. (2010). Subpolar link to the emergence of the modern equatorial Pacific cold tongue. *Science*, *328*, 1550–1553. https://doi.org/10.1126/science.1184480

McClymont, E. L., & Rosell-Melé, A. (2005). Links between the onset of modern Walker circulation and the mid-Pleistocene climate transition. *Geology*, *33*, 389–392. https://doi.org/10.1130/G21292.1

McClymont, E. L., Sosdian, S. M., Rosell-Melé, A., & Rosenthal, Y. (2013). Pleistocene sea-surface temperature evolution: Early cooling, delayed glacial intensification, and implications for the mid-Pleistocene climate transition. *Earth Science Reviews*, *123*, 173–193. https://doi.org/10.1016/j.earscirev.2013.04.006

Mitchell, T. P., & Wallace, J. M. (1992). The annual cycle in equatorial convection and sea surface temperature. *Journal of Climate*, *5*(10), 1140–1156. https://doi.org/10.1175/1520-0442(1992)005<1140:TACIEC>2.0.CO;2

Mortlock, R. A., & Froelich, P. N. (1989). A simple method for the rapid determination of biogenic opal in pelagic marine sediments. *Deep-Sea Research*, *36*(9), 1415–1426. https://doi.org/10.1016/0198-0149(89)90092-7

Pena, L. D., Cacho, I., Ferretti, P., & Hall, M. A. (2008). ENSO-like variability during glacial terminations and interlatitudinal teleconnections. *Paleoceanography*, *23*, PA3101. https://doi.org/10.129/2008PA001620

Pena, L. D., & Goldstein, S. L. (2014). Thermohaline circulation crisis and impacts during the mid-Pleistocene transition. *Science*, *345*, 318–322. https://doi.org/10.1126/science.1249770

Pennington, J. T., Mahoney, K. L., Kuwahara, V. S., Kolber, D. D., Calienes, R., & Chaves, F. P. (2006). Primary production in the eastern tropical Pacific: A review. *Progress in Oceanography*, *69*, 285–317. https://doi.org/10.1016/j.pocean.2006.03.012

Philander, S. G., & Fedorov, A. V. (2003). Role of tropics in changing the response to Milankovich forcing some three million years ago. *Paleoceanography*, *18*(2), 1045. https://doi.org/10.1029/2002PA000837

Rafter, P. A., & Charles, C. (2012). Pleistocene equatorial Pacific dynamics inferred from the zonal asymmetry in sedimentary nitrogen isotopes. *Paleoceanography*, *27*, PA3102. https://doi.org/10.1029/2012PA002367

Rafter, P. A., DiFiore, P. J., & Sigman, D. M. (2013). Coupled nitrate nitrogen and oxygen isotopes and organic matter remineralization in the Southern and Pacific Oceans. *Journal of Geophysical Research: Oceans*, *118*, 4781–4794. https://doi.org/10.1002/jgrc.20316

Rafter, P. A., Sigman, D. M., Charles, C. D., Kaiser, J., & Haug, G. H. (2012). Subsurface tropical Pacific nitrogen isotopic composition of nitrate: Biogeochemical signals and their transport. *Global Biogeochemical Cycles*, *26*, GB1003. https://doi.org/10.1029/2010GB003979

Rafter, P. A., Sigman, D. M., & Mackey, K. R. M. (2017). Recycled iron fuels new production in the eastern equatorial Pacific Ocean. *Nature Communications*, *8*, 1100. https://doi.org/10.1038/s41467-017-01219-7

Robinson, R. S., Etourneau, J., Martinez, P. M., & Schneider, R. (2014). Expansion of water column denitrification during early Pleistocene cooling. *Earth and Planetary Science Letters*, *389*, 52–61. https://doi.org/10.1016/j.epsl.2013.12.022

Robinson, R. S., Kienast, M., Albuquerque, A. L., Altabet, M., Contreras, S., Holz, R. D., et al. (2012). A review of nitrogen isotopic alteration in marine sediments. *Paleoceanography*, *27*, PA4203. https://doi.org/10.1029/2012PA002321

Robinson, R. S., Martinez, P., Pena, L. D., & Cacho, I. (2009). Nitrogen isotopic evidence for deglacial changes in nutrient supply in the eastern equatorial Pacific. *Paleoceanography*, *24*, PA4213. https://doi.org/10.1029/2008PA001702

Sarmiento, J. L., Gruber, N., Brzezinski, M. A., & Dunne, J. P. (2004). High-latitude controls of thermocline nutrients and low latitude biological productivity. *Nature*, *427*(6969), 56–60. https://doi.org/10.1038/nature02127

Schefuss, E., Schouten, S., Jansen, J. H. F., & Sinninghe Damsté, J. S. (2003). African vegetation controlled by tropical sea surface temperatures in the mid-Pleistocene period. *Nature*, *422*(6930), 418–421. https://doi.org/10.1038/nature01500

Seo, I., Lee, Y. I., Kim, W., Yoo, C. M., & Hyeong, K. (2015). Movement of the Intertropical Convergence Zone during the mid-Pleistocene transition and the response of atmospheric and surface ocean circulations in the central equatorial Pacific. *Geochemistry, Geophysics, Geosystems*, *16*, 3973–3981. https://doi.org/10.1002/2015GC006077

Shipboard-Scientific-Party (1992). *Site 846, proceedings of the Ocean Drilling Program Initial Reports*. College Station, TX: Ocean Drilling Program.

Sigman, D. M., Hain, M. P., & Haug, G. H. (2010). The polar ocean and glacial cycles in atmospheric CO_2 concentration. *Nature*, *466*, 47–55. https://doi.org/10.1038/nature09149

Spero, H. J., & Lea, D. W. (2002). The cause of carbon isotope minimum events on glacial terminations. *Science*, *296*(5567), 522–525. https://doi.org/10.1126/science.1069401

Toggweiler, J. R., Dixon, K., & Broecker, W. S. (1991). The Peru upwelling and the ventilation of the South-Pacific thermocline. *Journal of Geophysical Research*, *96*(C11), 20,467–20,497. https://doi.org/10.1029/91JC02063

Weltje, G. J., & Tjallingii, R. (2008). Calibration of XRF core scanners for quantitative geochemical logging of sediment cores: Theory and application. *Earth and Planetary Science Letters*, *274*, 423–438. https://doi.org/10.1016/j.epsl.2008.07.054

Winckler, G., Anderson, R. F., & Schlosser, P. (2005). Equatorial Pacific productivity and dust flux during the mid-Pleistocene climate transition. *Paleoceanography*, *20*, PA4025. https://doi.org/10.1029/2005PA001177